Environmental Science & Technology

pubs.acs.org/est

Article

Adsorption and Reductive Defluorination of Perfluorooctanoic Acid over Palladium Nanoparticles

Min Long, Juan Donoso, Manav Bhati, Welman C. Elias, Kimberly N. Heck, Yi-Hao Luo, YenJung Sean Lai, Haiwei Gu, Thomas P. Senftle, Chen Zhou,* Michael S. Wong, and Bruce E Rittmann

Cite This: *Environ. Sci. Technol.* 2021, 55, 14836−14843

Read Online

ACCESS | Metrics & More | Article Recommendations | Supporting Information

ABSTRACT: Per- and polyfluoroalkyl substances (PFASs) comprise a group of widespread and recalcitrant contaminants that are attracting increasing concern due to their persistence and adverse health effects. This study evaluated removal of one of the most prevalent PFAS, perfluorooctanoic acid (PFOA), in H_2-based membrane catalyst-film reactors (H_2-MCfRs) coated with palladium nanoparticles (Pd^0NPs). Batch tests documented that Pd^0NPs catalyzed hydrodefluorination of PFOA to partially fluorinated and nonfluorinated octanoic acids; the first-order rate constant for PFOA removal was 0.030 h^{-1}, and a maximum defluorination rate was 16 μM/h in our bench-scale MCfR. Continuous-flow tests achieved stable long-term depletion of PFOA to below the EPA health advisory level (70 ng/L) for up to 70 days without catalyst loss or deactivation. Two distinct mechanisms for Pd^0-based PFOA removal were identified based on insights from experimental results and density functional theory (DFT) calculations: (1) nonreactive chemisorption of PFOA in a perpendicular orientation on empty metallic surface sites and (2) reactive defluorination promoted by physiosorption of PFOA in a parallel orientation above surface sites populated with activated hydrogen atoms (H_{ads}*). Pd^0-based catalytic reduction chemistry and continuous-flow treatment may be broadly applicable to the ambient-temperature destruction of other PFAS compounds.

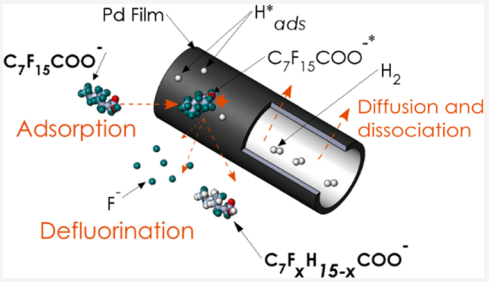

KEYWORDS: *perfluorooctanoic acid, palladium, adsorption, hydrodefluorination, catalysis*

INTRODUCTION

The widespread applications of PFASs (poly- and perfluorinated alkyl substances), a group of man-made chemicals,[1] have led to large-scale contamination of soil and groundwater throughout the world.[1,2] For example, perfluorooctanoic acid (PFOA), one of the most widely used PFAS compounds, has been used as a refrigerant, in fabrics and food packaging, and as a flame retardant at airports and military installations.[3] PFOA concentrations in natural waters typically are at ng/L levels,[4] PFOA concentrations in industrial wastewater can reach up to 1000 mg/L,[5] and groundwater contaminated by aqueous film-forming foams (AFFF) shows PFOA concentrations up to 6570 μg/L.[4] PFOA has negative impacts on human and ecosystem health and has been detected in blood serum.[6] Based on toxicity tests and risk assessments, the USEPA set a lifetime health advisory level at 70 ppt of combined PFOA and PFOS (perfluorooctanesulfonic acid) for drinking water.[7]

Adsorption and filtration are the most common approaches for removing PFASs from groundwater in practice today.[2] These approaches do not destroy PFASs but require further processing or disposal of the concentrated PFAS. Destroying PFASs or converting them to less toxic compounds would lower environmental and human health risks. The key challenge for destroying PFASs lies in their notorious recalcitrance that is linked to the high dissociation energy (440.99 kJ/mol) of the carbon−fluorine (C−F) bond.[8] Although biodegradation of some PFASs has been reported,[9−12] slow rates (typically over 100 days for substantial depletion or no F^- detected) hinder practical applications. Other destruction methods, such as sonication,[13] plasma treatment,[14] thermal treatment,[15] and chemical oxidation,[16] are able to break the C−F bonds, but they generally require high investment costs and a high requirement for energy, temperature, or pressure, and they often give rise to hazardous secondary pollution.[17] Only a few studies reported the alternative reductive defluorination using chemical reducing agents like ZVI (zero-valent iron)[18] or titanium(III) citrate[19,20] for PFAS removal. These reductive methods are hindered by low efficiency or activity, secondary contaminants, and poorly understood mechanisms.

A novel alternative is to use precious metals that are widely applied for catalyzing hydrodehalogenating reactions with controllable activity and selectivity.[21] Elemental palladium

Received: May 14, 2021
Published: September 9, 2021

(Pd^0) is most studied and has greater catalytic activities in dehalogenation than other precious metals.[22,23] Pd^0-catalyzed reductive defluorination of partially fluorinated arenes,[24] freons,[25] pharmaceuticals,[26] and allylic gem-difluorides[27] is well documented and points to the possibility of using Pd^0 catalysts to treat perfluorinated compounds.

In this study, we tested the hypothesis that PFOA can be efficiently destroyed via reductive defluorination over Pd^0 catalysts. Similar to other hydrodehalogenating processes, PFOA is adsorbed on the Pd^0 surface, and the F in each C−F bond is replaced by an adjacent activated H atom (H_{ads}*), which also is adsorbed on the Pd^0 surface via H_2 dissociation.[19] We conducted experiments on PFOA removal and defluorination in a bench-scale membrane catalyst-film reactor (MCfR), a platform that enables reliable, controllable, and high-efficiency (close to 100%[28]) delivery of H_2 in a bubble-free form by its diffusion through nonporous membranes onto which Pd^0 nanoparticles are spontaneously synthesized and deposited at ambient temperature and with high stability and longevity.[29] We investigated the roles of PFOA adsorption and H_2-driven defluorination using relatively high concentrations of PFOA in batch-mode MCfRs. We also evaluated long-term continuous removal of PFOA at environmentally relevant concentrations in a continuously operated MCfR.

MATERIALS AND METHODS

Reactor Setup. Figure S1 illustrates the bench-scale MCfR configuration, consisting of a 30 cm glass tube connected with plastic tubing through a recirculation pump (Masterflex, USA) that gave a recirculation rate of 150 mL/min (~6000 times the feeding rate during continuous-flow operation) and made the MCfR's liquid contents well mixed.[30,31] The tube had a bundle of 120 24-cm hollow-fiber membranes (polypropylene; Teijin, Ltd., Japan) with 200 μm OD, 100 μm ID, and wall thickness at 50 μm. It contained 181 cm^2 of the total membrane surface area and a 40 mL working volume. Ultrapure H_2 was supplied to both ends of the fiber bundles from a H_2 cylinder, with the pressure controlled by a H_2 regulator at 20 psig.

In Situ Synthesis and Deposition of Pd^0 Catalysts on the Membranes. The Pd^{2+} precursor solution contained 5 mM sodium tetrachloropalladate (Na_2PdCl_4) dissolved in deoxygenated deionized water (DI) at pH 7.0, controlled using a potassium phosphate buffer. We filled the MCfR with the precursor solution and then kept the MCfR in batch mode (i.e., no influent or effluent) for 24 h until <1% of Pd was left in the liquid phase. This yielded 1.6 ± 0.2 mg of Pd^0 loaded on the membrane surface, giving an average surface density of 0.9 ± 0.1 g/m^2. We then drained the liquid from the MCfR and rinsed the MCfR with DI water three times.

Batch Tests of Catalytic Defluorination of PFOA Using MCfRs. For initial batch tests, we set up two freshly prepared MCfRs and one reactor with bare membranes as a control. We supplied one of the MCfRs with N_2 and the other with H_2 to test the removal of PFOA via adsorption alone (N_2) and via adsorption plus defluorination (H_2). For the sequential-batch cycles, we also set up two MCfRs with H_2 and another with N_2; they were fed with 100 μM PFOA for three consecutively repeated batch cycles. We conducted each batch test in triplicate. Each batch cycle lasted for 45 h. The initial pH was buffered by adding 1.5 mM phosphate buffer.

To begin each batch test, the MCfR or control was purged with pure N_2 gas for 15 min to remove O_2, and then, the PFOA stock solution was rapidly (~10 s) introduced into the MCfR using a feeding pump. The batch test began once the MCfR or control was filled with the PFOA stock solution.

Single-Pass Flow Tests of Catalytic Defluorination of PFOA Using MCfRs. We set up two freshly prepared H_2-MCfRs, each having 0.9 g Pd^0/m^2, for continuous removal of ~500 ng/L PFOA supplied with a constant N_2 pressure of 20 psig (adsorption alone) or a constant H_2 pressure of 20 psig (adsorption and defluorination). The continuous-flow rate was 0.025 mL/min, which yielded a hydraulic retention time (HRT) of 24 h and a PFOA surface loading rate of 0.8 ± 0.06 $\mu g \cdot m^{-2} \cdot d^{-1}$. The maximum F^- release could have been 0.018 μM in the effluent, which was too low to be detected by IC (LOD at 0.5 μM).

Nanoparticle Collection and Solid-State Characterization. After the batch test, we cut several pieces of the membrane from the MCfR and prepared the samples based on our established protocol.[31] After fixation of these samples, we examined them using JEM-ARM200F scanning transmission electron microscopy (STEM) for imaging, crystallite diffraction, and lattice-fringe fingerprinting. X-ray photoelectron spectroscopy (XPS) of the fibers was carried out using a PHI Quantera SXM (ULVAC-PHI. Inc) with an Al source (a focused beam of 1.5 kV, 25 W). X-ray powder diffraction (XRD) was conducted with a Philips X'Pert Pro equipped with a Cu Kα radiation source (1.540598 Å). XRD analysis was conducted in a 2θ range of 10−90°, with a step size of 0.0050 s^{-1}.

Sampling and Analyses. We collected liquid samples from the MCfR using 3 mL syringes and immediately filtered the sample through a 0.22 μm PES membrane filter (NEST Scientific) (Figure S2, minimal loss).[32] F^- was analyzed using an ion chromatograph (IC-930, Metrohm, USA). PFOA (>0.1 μM, 0.04 ppm) was determined using ultraperformance liquid chromatography (UPLC) (Waters LC-20A, United States) with a Waters C18 column and an evaporative light scattering detector (ELSD). PFOA (at the ppt level) was determined using an Agilent 1290 UPLC system coupled to a 6490 triple quadrupole mass spectrometer system (QQQ-MS) based on the EPA Method 537.1.[33] Defluorination products from PFOA were analyzed using an Agilent 1290 high performance liquid chromatography system coupled to an Agilent 6530 quadrupole/time-of-flight mass spectrometer (HPLC-QTOF-MS) for qualitative analysis. Details of the analytical methods, including detection limits, are summarized in Section 1 of the Supporting Information.

Calculations. The PFOA removal ratio was calculated through eq 1:

$$\text{PFOA removal ratio} = \frac{C_0 - C_{PFOA}}{C_0} \quad (1)$$

where C_0 is the initial PFOA concentration and C_{PFOA} is the PFOA concentration (μM).

Defluorination ratio was calculated through eq 2:

$$\text{defluorination ratio} = \frac{C_F}{15(C_0 - C_{PFOA})} \quad (2)$$

where C_F is the fluoride ion concentration (μM).

The PFOA surface loading rate was calculated through eq 3:

$$\text{surface loading rate} = C_0 \frac{Q}{A} \quad (3)$$

https://doi.org/10.1021/acs.est.1c03134
Environ. Sci. Technol. 2021, 55, 14836−14843

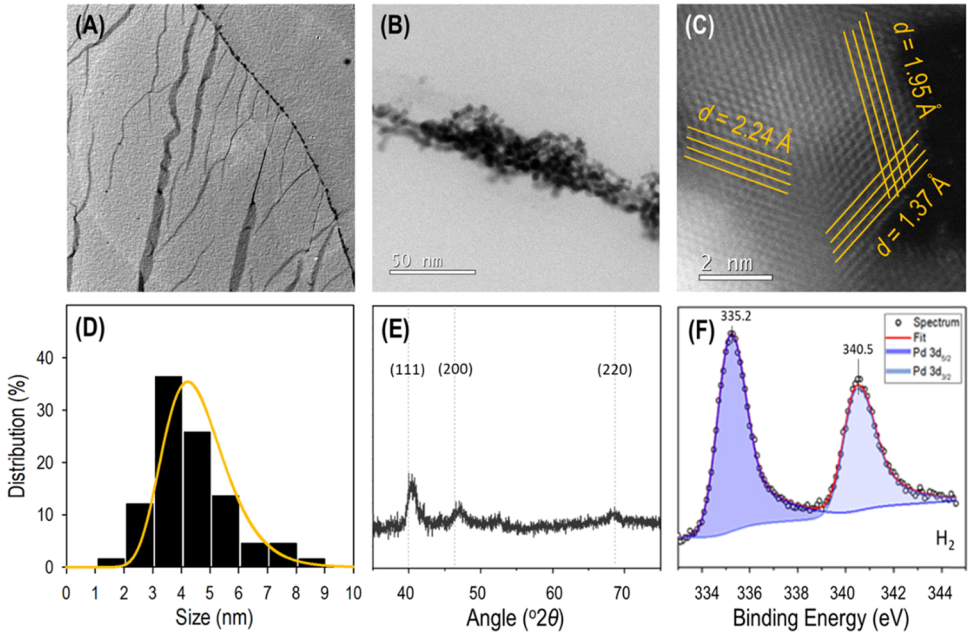

Figure 1. (A) TEM image of a cross-section of the Pd fiber. (B) TEM image of the boundary of the Pd fiber. (C) Lattice fingers of the nanoparticles. (D) Size distribution of the nanoparticles in figure (B). (E) XRD spectra of the Pd fiber. (F) XPS spectra of the Pd fiber.

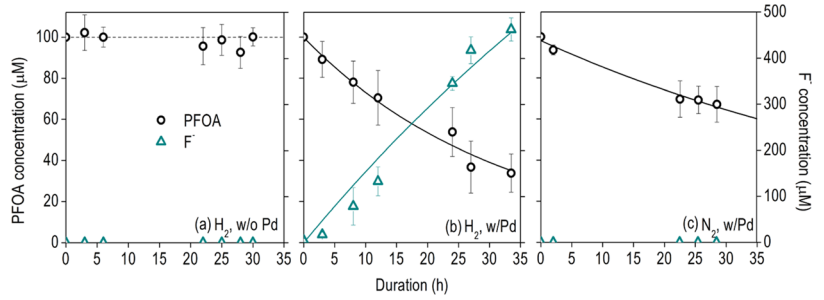

Figure 2. PFOA and F^- concentration changes over time during the 0.1 mM PFOA batch tests (a) without and (b) with the Pd catalyst (0.9 g/m^2 areal loading) for H_2 supply and (c) with the same loading of Pd^0 catalyst for N_2 supply. Reaction conditions: pH 4, 0.1 mM initial PFOA, and 150 mL/min recirculating flow rate.

where the surface loading rate is in the unit of $\mu g \cdot m^{-2} \cdot d^{-1}$; C is the concentration of influent PFOA (μg/L); Q is the flow rate (L/day); and A is the total fiber surface area (18.48×10^{-3} m^2).

Removal flux was calculated through eq 4:[31]

$$J_{pfoa} = (C_0 - C_{PFOA})\frac{Q}{A} \quad (4)$$

where J_{pfoa} is the removal flux for reducing PFOA ($\mu g \cdot m^{-2} \cdot d^{-1}$).

Computational Methods. We performed density functional theory (DFT) calculations to determine the PFOA adsorption modes on the most stable Pd (111) surface and to investigate the effect of surface hydrogen coverage on PFOA adsorption. On the Pd (111) surface, we calculated the adsorption energy of the PFOA molecule as

$$\Delta E^{ads}_{Pd/PFOA} = E_{Pd/PFOA} - E_{Pd} - E_{PFOA} \quad (5)$$

where $E_{Pd/PFOA}$ is the energy of PFOA adsorbed on Pd (111), E_{Pd} is the energy of the clean Pd (111) slab, and E_{PFOA} is the energy of the isolated PFOA molecule. DFT calculations were performed with the Vienna Ab initio Simulation Package[34,35] (VASP 5.4.4) in conjunction with the VASPsol implicit solvation model.[36,37] Detailed calculation methods are provided in Supporting Information Section 2.[38−45]

RESULTS AND DISCUSSION

Characteristics of Pd^0 Loaded on Membranes. Figure 1 presents the solid-state characteristics of the fiber samples loaded with 0.9 g/m^2 Pd^0 in the MCfR. The TEM images reveal that Pd^0 homogeneously anchored on the membrane surface, almost a complete continuous film: The film was 10−20 nm thick (Figure 1A) and composed of stacked nanoparticles (Figure 1B) featuring lattice spacings of 1.37, 1.95, and 2.24 Å (Figure 1C) corresponding to the (220), (200), and (111) planes of typical face-centered cubic (FCC) Pd^0.[46] These Pd^0NPs had an average size of 4.2 nm (Figure 1D), which is similar to those in previous MCfRs.[31,47] The XRD pattern further verified the presence of crystalline Pd^0, with three characteristic diffraction peaks at 40.4, 47.0, and 68.4°, with d-spacing values of 1.37, 1.93, and 2.23 corresponding to (111), (200), and (220) planes, respectively, similar values are obtained by the lattice spaces on the micrograph from Figure 1C. A crystallite size of 5.9 nm was estimated using the Scherrer equation. XPS analysis (Figure 1F) reveals only the existence of one peak at $Pd_{3/2}$ and $Pd_{5/2}$

https://doi.org/10.1021/acs.est.1c03134
Environ. Sci. Technol. 2021, 55, 14836−14843

energy, centered at 340.5 and 335.3 eV, which indicates the presence of only Pd^0.[48,49]

Batch Tests of PFOA Removal over Pd^0: Adsorption and Defluorination Mechanisms. Figures 234 show the

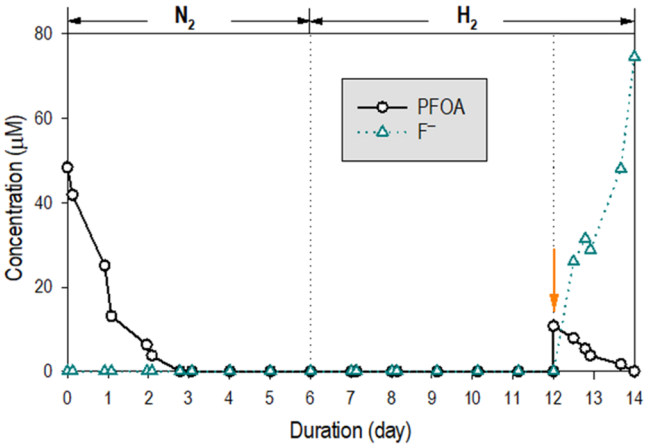

Figure 3. PFOA and F^- concentrations over time in the extended batch test for 0.9 g/m^2 Pd^0 at pH 4 in the MCfR supplied with 20 psig N_2 for 6 days followed by 20 psig H_2 for 8 days. The orange arrow refers to PFOA respiking into the liquid in the MCfR on day 12.

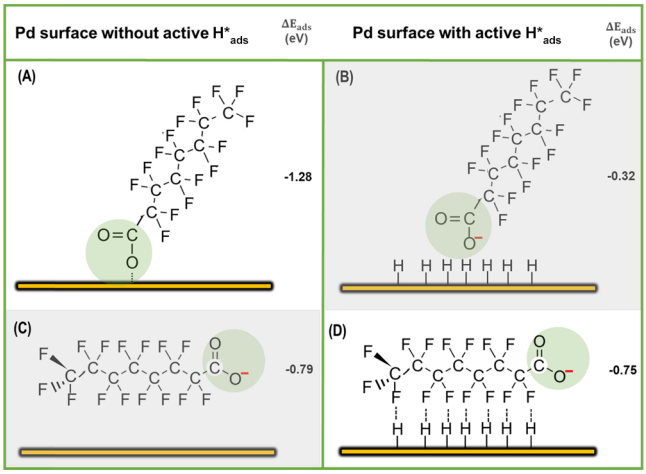

Figure 4. Proposed two distinct adsorption mechanisms of PFOA. Perpendicular (non-defluorinative) and parallel (defluorinative) adsorption modes of PFOA to the Pd (111) surface under different conditions along with respective adsorption energies (in eV). Shaded adsorption modes represent the less favorable mode for each condition. The gold lines represent Pd^0 surfaces. The H connected on Pd^0 represents activated H*. The green circles identify PFOA's carboxyl heads.

experimental results for the batch tests of PFOA depletion in the MCfRs. The default conditions included 0.9 g/m^2 Pd^0, 0.1 mM initial PFOA, pH 4, and constant 20 psig (2.36 atm absolute) gas pressure.

Pd^0-Catalyzed Reductive Defluorination of PFOA in the Presence of H_2. In the absence of Pd^0 (i.e., bare membranes with H_2 supply; Figure 2A), the PFOA concentration had minimal decrease (less than 8%) over 35 h (Figure 2A), indicating that PFOA had negligible reaction with the polypropylene membranes or other materials composing the MCfR. With ~0.9 g/m^2 Pd^0NPs loaded on the membrane surface and the same H_2 supply, 66 ± 9% of the PFOA was depleted within 35 h (Figure 2B), along with gradual release of free fluoride ions (F^-) up to 0.46 ± 0.02 mM (accounting for 46 ± 2% of all F in the depleted PFOA).

HPLC-QTOF-MS analyses (Figure S3 in the Supporting Information) reveal that while PFOA ($C_8HO_2F_{15}$) was the only fluorinated carboxylic acid ($C_aH_bO_2F_d$) detected initially, at least four partially fluorinated octanoic acid (OA) species ($C_8H_2F_{14}O_2$, $C_8H_3F_{13}O_2$, $C_8H_7F_9O_2$, and $C_8H_8F_8O_2$) and nonfluorinated OA ($C_8H_{16}O_2$) were identified in the bulk liquid of the H_2-MCfR after 35 h.

These results verify our hypothesis and document for the first time that Pd^0 is capable of catalyzing reductive defluorination of PFOA into partial or nonfluorinated OAs. The HPLC-QTOF-MS results suggest that the following reactions occurred:

$$C_8HF_{15}O_2 + 2H_{ads}^* \rightarrow C_8H_2F_{14}O_2 + F^- + H^+ \quad (6)$$

$$C_8HF_{15}O_2 + 4H_{ads}^* \rightarrow C_8H_3F_{13}O_2 + 2F^- + 2H^+ \quad (7)$$

$$C_8HF_{15}O_2 + 12H_{ads}^* \rightarrow C_8H_7F_9O_2 + 6F^- + 6H^+ \quad (8)$$

$$C_8HF_{15}O_2 + 14H_{ads}^* \rightarrow C_8H_8F_8O_2 + 7F^- + 7H^+ \quad (9)$$

$$C_8HF_{15}O_2 + 30H_{ads}^* \rightarrow C_8H_{16}O_2 + 15F^- + 15H^+ \quad (10)$$

Although the medium was buffered, the pH decreased from 4.0 ± 0.1 to 3.8 ± 0.06 after the reactions, verifying the occurrence of the defluorination that produced H^+.

Non-defluorinative Adsorption of PFOA on Pd^0 in the Absence of H_2. When H_2 was replaced by N_2 at the same pressure of 20 psig, we detected 33 ± 8% PFOA removal but no F^- release within 30 h (Figure 2C). No partially defluorinated carboxylic acids were detected by HPLC-QTOF-MS. These results reveal that in the absence of H_2 as the electron donor, no defluorination or other chemical reactions occurred, but the H_{ads}*-free Pd^0 still was able to adsorb PFOA.

To explore further this observation of PFOA adsorption on H_{ads}*-free Pd, we carried out an extended 2 week batch test (Figure 3). Over 99.9% of the initial 0.05 mM PFOA was adsorbed by Pd^0 within 67 h under N_2. After 6 days, we replaced N_2 with H_2 but did not observe F^- release for the following 6 days. This suggests that the adsorbed PFOA on the H_{ads}*-free Pd^0 surface was not able to be defluorinated in the presence of H_2. We then respiked 0.01 mM PFOA and observed >99% PFOA removal along with 46% defluorination within 50 h. This implies that Pd^0 still had active sites available for H_{ads}*, and H_{ads}* was able to defluorinate newly introduced PFOA from the bulk liquid, but not PFOA already adsorbed prior to the presence of H_{ads}*.

Mechanistic Interpretation of the Batch Results. Overall, the batch results identified two distinct adsorption patterns involved in PFOA removal by Pd^0: H_{ads}*-independent nonreactive adsorption and H_{ads}*-dependent reactive (defluorinating) adsorption. We propose that the two adsorption patterns are associated not only with the presence of H_{ads}* but also with different adsorptive positions and orientations.

The hypothesis of different adsorption orientations is based on DFT modeling, whose results are summarized in Figure 4. Because the reported pK_a values for PFOA are ≤2.8,[50,51] PFOA predominantly exists in the deprotonated form as the $C_7F_{15}COO^-$ anion. DFT calculations reveal that when H_2 is absent (Figure 4A,C), $C_7F_{15}COO^-$ tends to bind to active Pd^0

https://doi.org/10.1021/acs.est.1c03134
Environ. Sci. Technol. 2021, 55, 14836−14843

sites in a perpendicular orientation, because of its more favorable adsorption energy ($\Delta E^{ads}_{Pd/PFOA}$= −1.28 eV) when a metal−oxygen bond can form compared to a parallel orientation ($\Delta E^{ads}_{Pd/PFOA}$= −0.79 eV), characteristic of physisorption. The nonreactive adsorption occurs through the carboxylate head group of PFOA binding via chemisorption by the formation of a Pd−O complex. The tail group is oriented off the surface, which keeps C−F bonds away from the Pd surface and thus minimizes chances of contact-based hydrodefluorination even when H_{ads}* is introduced.

In contrast, when H_2 is present (Figure 4BD), the high amounts of H_{ads}* on the surface block Pd−O bond formation, which favors parallel binding orientation ($\Delta E^{ads}_{Pd/PFOA}$= −0.75 eV, compared to −0.32 eV for the perpendicular orientation) through van der Waals attraction. Parallel adsorption allows maximum contact of C−F bonds and H_{ads}* on the Pd^0 surface, which promotes catalytic reduction of PFOA via surface H addition or F/H substitution. After the reaction, defluorinated products and fluoride desorb from the Pd surface,[19,52] which frees Pd^0 active sites for continued defluorinative adsorption of PFOA. This DFT-based atomistic-scale insight into PFOA adsorption on the Pd^0 surface agrees with the adsorption trends observed experimentally.

Long-Term Tests on PFOA Removal over Pd^0: Efficiency and Longevity. *Sequential-Batch Tests.* Figure 5 shows the experimental results for three successive cycles of batch tests in which 100 μM PFOA was applied in each cycle to each of the two MCfRs loaded with 0.9 g/m^2 Pd^0 but supplied with different gases. In the N_2-MCfR (Figure 5A), 41 ± 1% of the PFOA was steadily depleted within 45 h in Cycle 1, which was similar to the N_2-MCfR before, but PFOA removal slowed and then stopped after 10 h in Cycle 2, and it was negligible in Cycle 3; this shows that the Pd^0 surface had become saturated with PFOA adsorbed on nonreactive sites by Cycle 2.

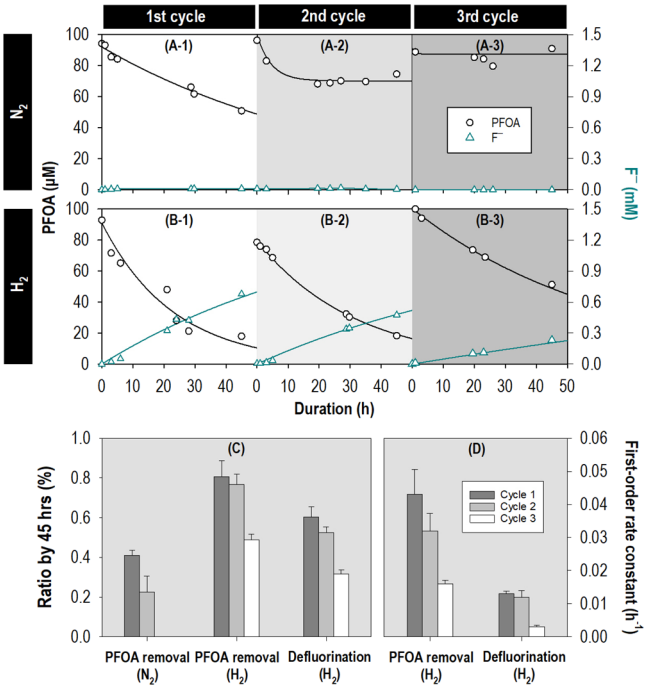

Figure 5. PFOA and F$^-$ concentrations over time in the sequential-batch tests for 0.9 g/m^2 Pd at pH 4 in two MCfRs supplied with 20 psig N_2 (A) and H_2 (B), respectively.

When H_2 was supplied (Figure 5B), over 80 ± 8% of the applied PFOA was depleted within 45 h in Cycle 1, along with 0.6 ± 0.05 mM F$^-$ release (58 ± 5% defluorination ratio). The PFOA removal rate and the defluorination ratio were similar to previous experiments with fresh Pd^0 (Figure 2). In the following two cycles, PFOA still was depleted, although the removal ratios decreased to 75 ± 5 and 47 ± 3%, along with decreased defluorination ratios of 52 ± 3 and 31 ± 2%, respectively (Figure 5C). On the one hand, the results reinforce that PFOA in the H_2-MCfR was mainly removed through defluorinative adsorption that led to the desorption of F$^-$ and defluorinated products,[19,52] which freed the active site with H_{ads}* for further reductive defluorination of PFOA from the bulk liquid. On the other hand, the gradual slowing of PFOA removal and defluorination rates (Figure 5D) suggests that active sites were becoming deactivated, probably due to the co-occurrence of non-defluorinative adsorption along with the defluorinative adsorption of PFOA. In order to maintain defluorinative activities for persistent PFOA depletion, non-defluorinative adsorption of PFOA needs to be minimized.

70 Day Continuous Tests. Figure 6 shows PFOA removals in two MCfRs operated in parallel with continuous flow over 70 days but with either N_2 or H_2 delivered to the membranes. Both MCfRs were continuously fed with ∼500 ppt of PFOA at the same flow rate of 0.025 mL/min (or an HRT of 24 h). The default conditions included 0.9 g/m^2 Pd^0 and constant 20 psig (or 2.36 atm absolute) gas pressure.

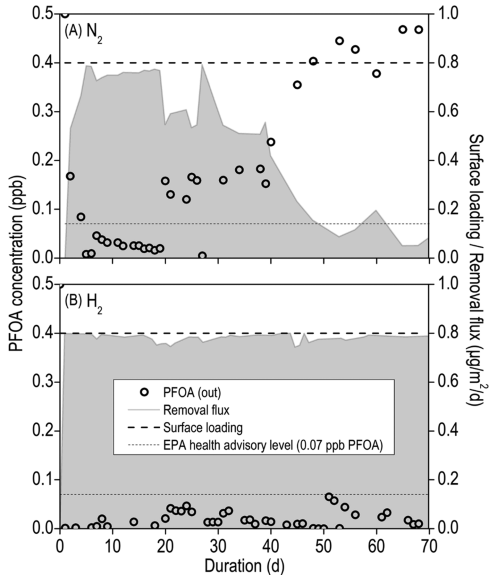

Figure 6. Concentrations of PFOA and F$^-$ in the effluents of two continuously operated MCfRs loaded with identical 0.9 mg/m^2 Pd^0NPs and supplied with 20 psig N_2 and H_2, respectively.

In the N_2-MCfR (Figure 6A), it took more than 5 days to achieve 99% of PFOA removal, and the effluent concentration of PFOA remained lower than the EPA health advisory level (70 ng/L) for the following 15 days. After 15 days, however, the effluent concentration of PFOA began to gradually increase and eventually was close the influent concentration after day 45. This trend is similar to the results with the sequential-batch tests (Figure 5A) and confirms that without H_2, exclusive non-defluorinative adsorption of PFOA on the Pd^0 surface became

https://doi.org/10.1021/acs.est.1c03134
Environ. Sci. Technol. 2021, 55, 14836−14843

saturated. According to the breakthrough curve (Figure S4), the total PFOA being adsorbed was 0.59 μg in 70 days. Although adsorption continued, the total removal of PFOA was much lower than the batch tests with 8000-fold higher influent concentration.

The H_2-MCfR achieved 99% PFOA removal within 1 day, and the effluent PFOA concentrations were consistently 20 ± 16 ng/L (i.e., less than one-third of the EPA health advisory level) throughout the 70 days of continuous operation. The total PFOA removed in the H_2-MCfR was 1.34 μg in 70 days, which was 128% greater than the removal in the N_2-MCfR. The minimal deactivation of the Pd^0 catalyst suggests that accumulation of nonreactively adsorbed PFOA was not important due to the constantly low concentration of PFOA in the MCfR.

■ ENVIRONMENTAL IMPLICATIONS

This study is the first report of Pd^0-catalyzed defluorination of perfluorinated compounds. Fast adsorption of PFOA and the release of F^- and partially and fully defluorinated compounds verified that the H_2-MCfR catalytically removed and destroyed PFOA. Defluorination preceded by PFOA adsorption in a parallel orientation that enabled the reaction between F substituents on PFOA and activated H on the Pd^0 surface. Operating under a continuous flow, the MCfR was capable of sustained removal of PFOA at environmentally relevant concentrations, averaging 97% removal to well below 70 ng/L for more than 2 months.

This success is based on efficient H_2 delivery in the MCfR. In contrast to conventional heterogeneous catalysis, the MCfR's nonporous membrane delivers H_2 directly to the film of Pd^0NPs. Direct delivery ensures that H* is always amply present at the Pd^0 surface, which minimizes vertical, non-defluorinative adsorption of PFOA and promotes parallel defluorinative desorption.

In the MCfR, PFOA was defluorinated to less- or nonfluorinated octanoic acids in the presence of H_2 as the electron donor:

$$C_7F_{15}COOH + nH_2 \rightarrow C_7H_nF_{15-n}COOH + nH^+ + nF^- \quad (1 \le n \le 15) \qquad (11)$$

The partially defluorinated and nonfluorinated compounds generating from Pd^0NP's catalytic defluorination of PFOA are more bioavailable and can be further biodegraded by aerobic bacteria,[53,54] possibly yielding complete mineralization to CO_2:

$$C_7H_nF_{15-n}COOH + (n + 29)/4O_2 \rightarrow 8CO_2 + (n + 1)/2H_2O + (15 - n)F^- \quad (1 \le n \le 15) \qquad (12)$$

Therefore, catalytic defluorination using the MCfR platform opens up a door for efficient and thorough treatment of PFAS-contaminated water when it is used synergistically with biodegradation.

■ ASSOCIATED CONTENT

Supporting Information

The Supporting Information is available free of charge at https://pubs.acs.org/doi/10.1021/acs.est.1c03134.

Chromatographic methods; DFT computational methods; photographic and schematic images of the bench-scale MCfR system; PFOA concentrations before and after filtration; HPLC-QTOF-MS results for Pd^0-catalyzed reduction of PFOA; and breakthrough curve for non-defluorinative adsorption of PFOA on Pd^0NPs in an MCfR (PDF)

■ AUTHOR INFORMATION

Corresponding Author

Chen Zhou − *Biodesign Swette Center for Environmental Biotechnology, Arizona State University, Tempe, Arizona 85287-5701, United States; Nanosystems Engineering Research Center for Nanotechnology-Enabled Water Treatment, Houston, Texas 77005, United States;* orcid.org/0000-0002-8104-2848; Email: zhou_SCEB@asu.edu

Authors

Min Long − *Biodesign Swette Center for Environmental Biotechnology, Arizona State University, Tempe, Arizona 85287-5701, United States; Nanosystems Engineering Research Center for Nanotechnology-Enabled Water Treatment, Houston, Texas 77005, United States;* orcid.org/0000-0001-5328-7787

Juan Donoso − *Nanosystems Engineering Research Center for Nanotechnology-Enabled Water Treatment, Houston, Texas 77005, United States; Department of Chemical and Biomolecular Engineering, Rice University, Houston, Texas 77005-1892, United States*

Manav Bhati − *Nanosystems Engineering Research Center for Nanotechnology-Enabled Water Treatment, Houston, Texas 77005, United States; Department of Chemical and Biomolecular Engineering, Rice University, Houston, Texas 77005-1892, United States*

Welman C. Elias − *Department of Chemical and Biomolecular Engineering, Rice University, Houston, Texas 77005-1892, United States*

Kimberly N. Heck − *Nanosystems Engineering Research Center for Nanotechnology-Enabled Water Treatment, Houston, Texas 77005, United States; Department of Chemical and Biomolecular Engineering, Rice University, Houston, Texas 77005-1892, United States*

Yi-Hao Luo − *Biodesign Swette Center for Environmental Biotechnology, Arizona State University, Tempe, Arizona 85287-5701, United States;* orcid.org/0000-0001-8975-8579

YenJung Sean Lai − *Biodesign Swette Center for Environmental Biotechnology, Arizona State University, Tempe, Arizona 85287-5701, United States*

Haiwei Gu − *Arizona Metabolomics Laboratory, College of Health Solutions, Arizona State University, Phoenix, Arizona 85004, United States;* orcid.org/0000-0002-7598-5022

Thomas P. Senftle − *Nanosystems Engineering Research Center for Nanotechnology-Enabled Water Treatment, Houston, Texas 77005, United States; Department of Chemical and Biomolecular Engineering, Rice University, Houston, Texas 77005-1892, United States;* orcid.org/0000-0002-5889-5009

Michael S. Wong − *Nanosystems Engineering Research Center for Nanotechnology-Enabled Water Treatment, Houston, Texas 77005, United States; Department of Chemical and Biomolecular Engineering, Rice University, Houston, Texas 77005-1892, United States;* orcid.org/0000-0002-3652-3378

Bruce E Rittmann − *Biodesign Swette Center for Environmental Biotechnology, Arizona State University,*

https://doi.org/10.1021/acs.est.1c03134
Environ. Sci. Technol. 2021, 55, 14836−14843

Tempe, Arizona 85287-5701, United States; Nanosystems Engineering Research Center for Nanotechnology-Enabled Water Treatment, Houston, Texas 77005, United States

Complete contact information is available at: https://pubs.acs.org/10.1021/acs.est.1c03134

Notes

The authors declare no competing financial interest.

■ ACKNOWLEDGMENTS

This work was partially supported by the National Science Foundation Engineering Research Center for Nanotechnology Enabled Water Treatment (EEC-1449500), the Strategic Environmental Research and Development Program (SERDP) (ER20-C1-1286), and Xylem Inc. (FP00019503). We acknowledge the use of facilities within the Eyring Materials Center and Mass Spectrometry at Arizona State University and the staff scientist involved in the data collection.

■ REFERENCES

(1) Moody, C. A.; Field, J. A. Perfluorinated surfactants and the environmental implications of their use in fire-fighting foams. *Environ. Sci. Technol.* **2000**, *34*, 3864−3870.

(2) Mahinroosta, R.; Senevirathna, L. A review of the emerging treatment technologies for PFAS contaminated soils. *J. Environ. Manage.* **2020**, *255*, No. 109896.

(3) Rahman, M. F.; Peldszus, S.; Anderson, W. B. Behaviour and fate of perfluoroalkyl and polyfluoroalkyl substances (PFASs) in drinking water treatment: a review. *Water Res.* **2014**, *50*, 318−340.

(4) Cheng, J.; Vecitis, C. D.; Park, H.; Mader, B. T.; Hoffmann, M. R. Sonochemical degradation of perfluorooctane sulfonate (PFOS) and perfluorooctanoate (PFOA) in landfill groundwater: environmental matrix effects. *Environ. Sci. Technol.* **2008**, *42*, 8057−8063.

(5) Rattanaoudom, R.; Visvanathan, C.; Boontanon, S. K. Removal of concentrated PFOS and PFOA in synthetic industrial wastewater by powder activated carbon and hydrotalcite. *J. Water Sustain.* **2012**, *2*, 245−258.

(6) Olsen, G. W.; Mair, D. C.; Lange, C. C.; Harrington, L. M.; Church, T. R.; Goldberg, C. L.; Herron, R. M.; Hanna, H.; Nobiletti, J. B.; Rios, J. A.; Reagen, W. K.; Ley, C. A. Per-and polyfluoroalkyl substances (PFAS) in American Red Cross adult blood donors, 2000−2015. *Environ. Res.* **2017**, *157*, 87−95.

(7) USEPA, Fact sheet: PFOA & PFOS drinking water health advisories (accessed April, 2018). https://www.epa.gov/ground-water-and-drinking-water/drinking-water-health-advisories-pfoa-and-pfos, 2016.

(8) O'Hagan, D. Understanding organofluorine chemistry. An introduction to the C−F bond. *Chem. Soc. Rev.* **2008**, *37*, 308−319.

(9) Huang, S.; Jaffé, P. R. Defluorination of perfluorooctanoic acid (PFOA) and perfluorooctane sulfonate (PFOS) by Acidimicrobium sp. strain A6. *Environ. Sci. Technol.* **2019**, *53*, 11410−11419.

(10) Liou, J.-C.; Szostek, B.; DeRito, C.; Madsen, E. Investigating the biodegradability of perfluorooctanoic acid. *Chemosphere* **2010**, *80*, 176−183.

(11) Wang, N.; Szostek, B.; Buck, R. C.; Folsom, P. W.; Sulecki, L. M.; Gannon, J. T. 8-2 Fluorotelomer alcohol aerobic soil biodegradation: Pathways, metabolites, and metabolite yields. *Chemosphere* **2009**, *75*, 1089−1096.

(12) Kwon, B. G.; Lim, H.-J.; Na, S.-H.; Choi, B.-I.; Shin, D.-S.; Chung, S.-Y. Biodegradation of perfluorooctanesulfonate (PFOS) as an emerging contaminant. *Chemosphere* **2014**, *109*, 221−225.

(13) Kucharzyk, K. H.; Darlington, R.; Benotti, M.; Deeb, R.; Hawley, E. Novel treatment technologies for PFAS compounds: A critical review. *J. Environ. Manage.* **2017**, *204*, 757−764.

(14) Singh, R. K.; Fernando, S.; Baygi, S. F.; Multari, N.; Thagard, S. M.; Holsen, T. M. Breakdown products from perfluorinated alkyl substances (PFAS) degradation in a plasma-based water treatment process. *Environ. Sci. Technol.* **2019**, *53*, 2731−2738.

(15) Watanabe, N.; Takata, M.; Takemine, S.; Yamamoto, K. Thermal mineralization behavior of PFOA, PFHxA, and PFOS during reactivation of granular activated carbon (GAC) in nitrogen atmosphere. *Environ. Sci. Pollut. Res.* **2018**, *25*, 7200−7205.

(16) Dombrowski, P. M.; Kakarla, P.; Caldicott, W.; Chin, Y.; Sadeghi, V.; Bogdan, D.; Barajas-Rodriguez, F.; Chiang, S. Y. Technology review and evaluation of different chemical oxidation conditions on treatability of PFAS. *Remediation* **2018**, *28*, 135−150.

(17) Merino, N.; Qu, Y.; Deeb, R. A.; Hawley, E. L.; Hoffmann, M. R.; Mahendra, S. Degradation and removal methods for perfluoroalkyl and polyfluoroalkyl substances in water. *Environ. Eng. Sci.* **2016**, *33*, 615−649.

(18) Liu, Y.; Ptacek, C. J.; Baldwin, R. J.; Cooper, J. M.; Blowes, D. W. Application of zero-valent iron coupled with biochar for removal of perfluoroalkyl carboxylic and sulfonic acids from water under ambient environmental conditions. *Sci. Total Environ.* **2020**, *719*, No. 137372.

(19) Lee, Y.-C.; Chen, Y.-P.; Chen, M.-J.; Kuo, J.; Lo, S.-L. Reductive defluorination of perfluorooctanoic acid by titanium (III) citrate with vitamin B12 and copper nanoparticles. *J. Hazard. Mater.* **2017**, *340*, 336−343.

(20) Sun, Z.; Geng, D.; Zhang, C.; Chen, J.; Zhou, X.; Zhang, Y.; Zhou, Q.; Hoffmann, M. R. Vitamin B12 (CoII) initiates the reductive defluorination of branched perfluorooctane sulfonate (br-PFOS) in the presence of sulfide. *Chem. Eng. J.* **2021**, *423*, No. 130149.

(21) Gichumbi, J. M.; Friedrich, H. B. Half-sandwich complexes of platinum group metals (Ir, Rh, Ru and Os) and some recent biological and catalytic applications. *J. Organomet. Chem.* **2018**, *866*, 123−143.

(22) Wu, B.-Z.; Chen, H.-Y.; Wang, S. J.; Wai, C. M.; Liao, W.; Chiu, K. Reductive dechlorination for remediation of polychlorinated biphenyls. *Chemosphere* **2012**, *88*, 757−768.

(23) Luis Benítez, A. J.; Angel, G. D. Total hydrodechlorination of industrial transformer oil on metal-supported catalysts. *Chem. Eng. Commun.* **2009**, *196*, 1217−1226.

(24) Baumgartner, R.; Stieger, G. K.; McNeill, K. Complete hydrodehalogenation of polyfluorinated and other polyhalogenated benzenes under mild catalytic conditions. *Environ. Sci. Technol.* **2013**, *47*, 6545−6553.

(25) Lunin, V.; Lokteva, E. Catalytic hydrodehalogenation of organic compounds. *Russ. Chem. Bull.* **1996**, *45*, 1519−1534.

(26) Park, J.; An, S.; Jho, E. H.; Bae, S.; Choi, Y.; Choe, J. K. Exploring reductive degradation of fluorinated pharmaceuticals using Al2O3-supported Pt-group metallic catalysts: Catalytic reactivity, reaction pathways, and toxicity assessment. *Water Res.* **2020**, *185*, No. 116242.

(27) Narumi, T.; Tomita, K.; Inokuchi, E.; Kobayashi, K.; Oishi, S.; Ohno, H.; Fujii, N. Facile synthesis of fluoroalkenes by palladium-catalyzed reductive defluorination of allylic gem-difluorides. *Org. Lett.* **2007**, *9*, 3465−3468.

(28) Tang, Y.; Ziv-el, M.; Zhou, C.; Shin, J. H.; Ahn, C. H.; Meyer, K.; Candelaria, D.; Friese, D.; Overstreet, R.; Scott, R.; Rittmann, B. E. Bioreduction of nitrate in groundwater using a pilot-scale hydrogen-based membrane biofilm reactor. *Front. Environ. Sci. Eng.* **2010**, *4*, 280−285.

(29) Luo, Y.-H.; Zhou, C.; Bi, Y.; Long, X.; Wang, B.; Tang, Y.; Krajmalnik-Brown, R.; Rittmann, B. E. Long-term continuous co-reduction of 1, 1, 1-trichloroethane and trichloroethene over palladium nanoparticles spontaneously deposited on H_2-transfer membranes. *Environ. Sci. Technol.* **2021**, *55*, 2057−2066.

(30) Nerenberg, R.; Rittmann, B. Hydrogen-based, hollow-fiber membrane biofilm reactor for reduction of perchlorate and other oxidized contaminants. *Water Sci. Technol.* **2004**, *49*, 223−230.

(31) Zhou, C.; Wang, Z.; Ontiveros-Valencia, A.; Long, M.; Lai, C.-y.; Zhao, H.-p.; Xia, S.; Rittmann, B. E. Coupling of Pd nanoparticles and denitrifying biofilm promotes H_2-based nitrate removal with greater selectivity towards N_2. *Appl. Catal. B* **2017**, *206*, 461−470.

(32) Sörengård, M.; Franke, V.; Tröger, R.; Ahrens, L. Losses of poly- and perfluoroalkyl substances to syringe filter materials. *J. Chromatogr. A* **2020**, *1609*, No. 460430.
(33) Determination of Selected Perfluorinated Alkyl Acids in Drinking Water by Solid Phase Extraction and Liquid Chromatography/Tandem Mass Spectrometry (LC/MS/MS) https://cfpub.epa.gov/si/si_public_record_report.cfm?Lab=NERL&dirEntryId=198984&simpleSearch=1&searchAll=EPA%2F600%2FR-08%2F092
(34) Kresse, G.; Furthmüller, J. Efficient iterative schemes for ab initio total-energy calculations using a plane-wave basis set. *Phys. Rev. B* **1996**, *54*, 11169.
(35) Kresse, G.; Furthmüller, J. Efficiency of ab-initio total energy calculations for metals and semiconductors using a plane-wave basis set. *Comput. Mater. Sci.* **1996**, *6*, 15−50.
(36) Mathew, K.; Sundararaman, R.; Letchworth-Weaver, K.; Arias, T.; Hennig, R. G. Implicit solvation model for density-functional study of nanocrystal surfaces and reaction pathways. *J. Chem. Phys.* **2014**, *140*, No. 084106.
(37) Mathew, K.; Kolluru, V. C.; Mula, S.; Steinmann, S. N.; Hennig, R. G. Implicit self-consistent electrolyte model in plane-wave density-functional theory. *J. Chem. Phys.* **2019**, *151*, 234101.
(38) Perdew, J. P.; Burke, K.; Ernzerhof, M. Generalized gradient approximation made simple. *Phys. Rev. Lett.* **1996**, *77*, 3865.
(39) Kresse, G.; Joubert, D. From ultrasoft pseudopotentials to the projector augmented-wave method. *Phys. Rev. B* **1999**, *59*, 1758.
(40) Monkhorst, H. J.; Pack, J. D. Special points for Brillouin-zone integrations. *Phys. Rev. B* **1976**, *13*, 5188.
(41) Methfessel, M.; Paxton, A. High-precision sampling for Brillouin-zone integration in metals. *Phys. Rev. B* **1989**, *40*, 3616.
(42) Grimme, S.; Antony, J.; Ehrlich, S.; Krieg, H. A consistent and accurate ab initio parametrization of density functional dispersion correction (DFT-D) for the 94 elements H-Pu. *J. Chem. Phys.* **2010**, *132*, 154104.
(43) Gauthier, J. A.; Ringe, S.; Dickens, C. F.; Garza, A. J.; Bell, A. T.; Head-Gordon, M.; Nørskov, J. K.; Chan, K. Challenges in modeling electrochemical reaction energetics with polarizable continuum models. *ACS Catal.* **2019**, *9*, 920−931.
(44) Van den Bossche, M.; Skúlason, E.; Rose-Petruck, C.; Jónsson, H. Assessment of constant-potential implicit solvation calculations of electrochemical energy barriers for H_2 evolution on Pt. *J. Phys. Chem. C* **2019**, *123*, 4116−4124.
(45) Bhati, M.; Chen, Y.; Senftle, T. P. Density Functional Theory Modeling of Photo-electrochemical Reactions on Semiconductors: H2 Evolution on 3C-SiC. *J. Phys. Chem. C* **2020**, *124*, 26625−26639.
(46) Lim, B.; Jiang, M.; Tao, J.; Camargo, P. H.; Zhu, Y.; Xia, Y. Shape-controlled synthesis of Pd nanocrystals in aqueous solutions. *Adv. Funct. Mater.* **2009**, *19*, 189−200.
(47) Cai, Y.; Long, X.; Luo, Y.-H.; Zhou, C.; Rittmann, B. E. Stable dechlorination of Trichloroacetic Acid (TCAA) to acetic acid catalyzed by palladium nanoparticles deposited on H_2-transfer membranes. *Water Res.* **2021**, *192*, No. 116841.
(48) Elias, W. C.; Signori, A. M.; Zaramello, L.; Albuquerque, B. L.; de Oliveira, D. C.; Domingos, J. B. Mechanism of a Suzuki-type homocoupling reaction catalyzed by palladium nanocubes. *ACS Catal.* **2017**, *7*, 1462−1469.
(49) NIST. *X-ray Photoelectron Spectroscopy Database, NIST Standard Reference Database Number 20*. National Institute of Standards and Technology: Gaithersburg MD, 2000.
(50) Lyu, X.; Liu, X.; Sun, Y.; Ji, R.; Gao, B.; Wu, J. Transport and retention of perfluorooctanoic acid (PFOA) in natural soils: Importance of soil organic matter and mineral contents, and solution ionic strength. *J. Contam. Hydrol.* **2019**, *225*, 103477.
(51) Krafft, M. P.; Riess, J. G. Per-and polyfluorinated substances (PFASs): Environmental challenges. *Curr. Opin. Colloid Interface Sci.* **2015**, *20*, 192−212.
(52) Wu, Z.; Pan, T.; Chai, Y.; Ge, S.; Ju, Y.; Li, T.; Liu, K.; Lan, L.; Yip, A. C.; Zhang, M. Synthesis of palladium phosphides for aqueous phase hydrodechlorination: Kinetic study and deactivation resistance. *J. Catal.* **2018**, *366*, 80−90.
(53) Liu, J.; Mejia Avendaño, S. Microbial degradation of polyfluoroalkyl chemicals in the environment: a review. *Environ. Int.* **2013**, *61*, 98−114.
(54) Bourgeois, A.; Bergendahl, J.; Rangwala, A. Biodegradability of fluorinated fire-fighting foams in water. *Chemosphere* **2015**, *131*, 104−109.

https://doi.org/10.1021/acs.est.1c03134
Environ. Sci. Technol. 2021, 55, 14836−14843